Supplementary Information: Parallel Implementation of High-Fidelity Multiqubit Gates with Neutral Atoms

H. Levine,[1] A. Keesling,[1] G. Semeghini,[1] A. Omran,[1] T. T. Wang,[1,2] S. Ebadi,[1] H. Bernien,[3] M. Greiner,[1] V. Vuletić,[4] H. Pichler,[1,5] and M. D. Lukin[1]

[1]*Department of Physics, Harvard University, Cambridge, MA 02138, USA*
[2]*Department of Physics, Gordon College, Wenham, MA 01984, USA*
[3]*Pritzker School of Molecular Engineering, University of Chicago, Chicago, IL 60637, USA*
[4]*Department of Physics and Research Laboratory of Electronics, Massachusetts Institute of Technology, Cambridge, MA 02139, USA*
[5]*ITAMP, Harvard-Smithsonian Center for Astrophysics, Cambridge, MA 02138, USA*

RAMAN LASER

We drive transitions between our qubit states using a 795 nm Raman laser which is $2\pi \times 100$ GHz red-detuned from the $5S_{1/2}$ to $5P_{1/2}$ transition. We couple the laser into a fiber-based Mach-Zehnder intensity modulator (Jenoptik AM785) which is DC biased around minimum transmission. The modulator is driven at half the qubit frequency ($\omega_{01} = 2\pi \times 6.83$ GHz), resulting in sidebands at $\pm 2\pi \times 3.42$ GHz, while the carrier and higher order sidebands are strongly suppressed. This approach is passively stable on the timescale of one day without any active feedback, in contrast with other approaches to generate sidebands through phase modulation and then separate suppression of the carrier mode with free space optical cavities or interferometers.

The Raman laser is aligned along the array of atoms (co-aligned with the 8.5 G bias magnetic field) and is σ^+ polarized, such that the two sidebands coherently drive π transitions between the $F = 1$ and $F = 2$ ground state manifolds with a Rabi frequency of $\Omega = 2\pi \times 250$ kHz (Fig. S1a). The Raman drive light induces a differential light shift of $2\pi \times 20$ kHz on the qubit transition; we adjust the drive frequency of the intensity modulator to correct for this light shift when we apply a Raman pulse.

OPTICAL PUMPING INTO $|0\rangle$

We optically pump atoms into $|0\rangle = |5S_{1/2}, F = 1, m_F = 0\rangle$ using a Raman-assisted pumping scheme with an 8.5 G magnetic field. As illustrated in Fig. S1b, we begin by coarse pumping of atoms into all m_F states within the $|5S_{1/2}, F = 1\rangle$ manifold by shining resonant light on the $|5S_{1/2}, F = 2\rangle$ to $|5P_{3/2}, F = 2\rangle$ transition. We then apply a Raman π pulse at a detuning that drives population from $|F = 1, m_F = -1\rangle$ to $|F = 2, m_F = -1\rangle$. A second pulse drives population from $|F = 1, m_F = +1\rangle$ to $|F = 2, m_F = +1\rangle$. The process then repeats by again coarse pumping any population that was transferred to $F = 2$ back into the $F = 1$ manifold. The net effect of one cycle is to transfer a portion of the population in $|F = 1, m_F = \pm 1\rangle$ into $|F = 1, m_F = 0\rangle$. We repeat this cycle 70 times over a duration of 300 μs to achieve a $|0\rangle$ preparation fidelity of 99.3(1)%.

RYDBERG LASER SYSTEM

We couple atoms from $|1\rangle = |5S_{1/2}, F = 2, m_F = 0\rangle$ to $|r\rangle = |70S_{1/2}, m_J = -1/2\rangle$ through a two-color laser system at 420 nm and 1013 nm, described in [1]. The lasers are polarized to drive σ^- and σ^+ transitions, respectively, through the intermediate state $|6P_{3/2}\rangle$. In previous experiments using $|5S_{1/2}, F = 2, m_F = -2\rangle$ as the ground state level, selection rules ensured that only a single intermediate sublevel within $|6P_{3/2}\rangle$ and only a single Rydberg state could be coupled. Additionally, the combined two-photon transition was magnetically insensitive.

Coupling from $|1\rangle = |5S_{1/2}, F = 2, m_F = 0\rangle$ to Rydberg states, as in these experiments, adds a few complications. Firstly, multiple intermediate states are coupled and both $|70S_{1/2}, m_J = \pm 1/2\rangle$ sublevels within the Rydberg manifold can be reached. This requires working at a higher magnetic field to spectrally separate the $m_J = \pm 1/2$ Rydberg levels. In these experiments, we work at a magnetic field of 8.5 G such that the splitting between $m_J = \pm 1/2$ is $2\pi \times 23.8$ MHz. The matrix element is also reduced in the coupling from $|1\rangle$ to $|r\rangle$ while the laser scattering rate stays the same; additionally, the transition is now magnetically sensitive. Nonetheless, this scheme benefits from high-quality qubit states $|0\rangle$ and $|1\rangle$ within the ground state manifold which can be easily coupled with a Raman laser system and which preserve coherence in optical tweezers. We note that the sensitivity to electric fields is unchanged in this scheme, but we can bound drifting or fluctuating electric fields in that the Ryberg resonance varies by < 50 kHz [2].

CONSTRUCTING QUANTUM CIRCUITS FROM NATIVE SINGLE-QUBIT GATES

All pulse sequences shown in the main text are decomposed into pre-calibrated single-qubit gates (and, where indicated, global multi-qubit gates). The two single-qubit gates are $X(\pi/4)$, implemented globally on all

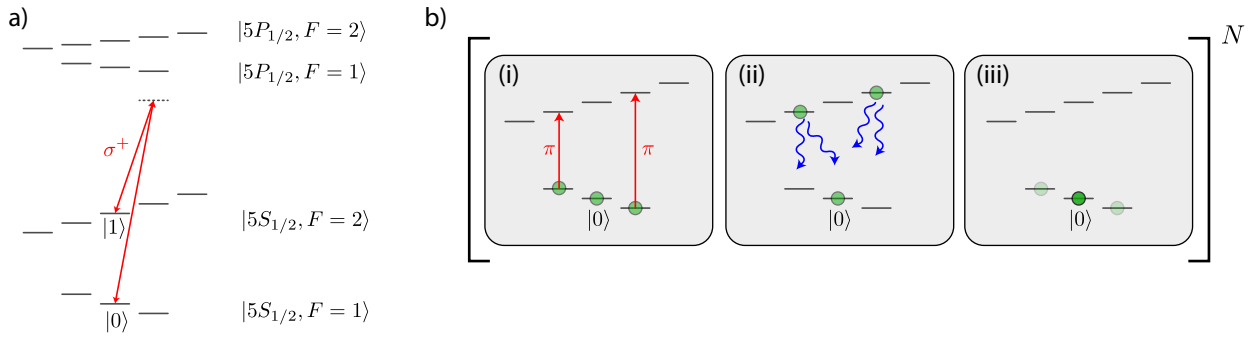

FIG. S1. **Raman laser and optical pumping.** a) Level diagram. The Raman laser is bichromatic and contains two frequency components separated by $2\pi \times 6.8$ GHz. These frequencies are red-detuned by $2\pi \times 100$ GHz to the $|5P_{1/2}\rangle$ manifold. b) Raman-assisted optical pumping. (i) We begin by coarse pumping into all three sublevels of $F = 1$, and apply a Raman π-pulse to excite from $|F = 1, m_F = -1\rangle$ to $|F = 2, m_F = -1\rangle$ and from $|F = 1, m_F = +1\rangle$ to $|F = 2, m_F = +1\rangle$. (ii) We then coarse pump back from $F = 2$ to $F = 1$. (iii) The net effect is to transfer some population from $|F = 1, m_F = \pm 1\rangle$ to $|F = 1, m_F = 0\rangle$. We repeat this cycle $N = 70$ times and achieve a net population of 99.3(1)% in $|0\rangle = |F = 1, m_F = 0\rangle$.

qubits simultaneously, and $Z(\pi)$, implemented by a light shift from a laser focused onto a single atom. In practice, the local $Z(\pi)$ gates are applied to one atom from each cluster at the same time (i.e., the left atom of each cluster or the middle of each cluster).

Initializing computational basis states

For two qubits, we initialize all four computational basis states using global $X(\pi/2)$ pulses (consisting of two sequential $X(\pi/4)$ gates) and local $Z(\pi)$ gates on the left atom only (top qubit in each circuit). The $|00\rangle$ state requires no pulses to prepare, and the $|11\rangle$ state requires only a global $X(\pi)$ gate. We prepare $|01\rangle$ as follows:

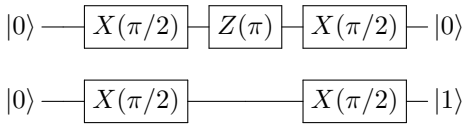

and $|10\rangle$ according to

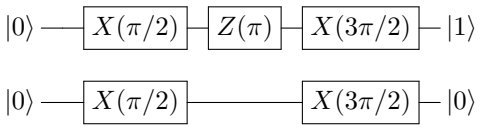

For three qubits, we initialize the eight computational basis states again using global $X(\pi/2)$ pulses and local $Z(\pi)$ pulses which can be applied to any of the three atoms. $|000\rangle$ and $|111\rangle$ can again be prepared with either no operation or with a global $X(\pi)$ gate, respectively. Other states have one atom in $|1\rangle$ and the other two in $|0\rangle$, or vice versa. We illustrate how both configurations are prepared by showing two examples. First, $|100\rangle$:

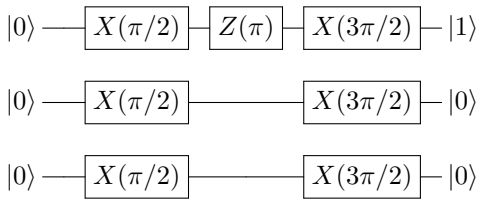

Next, we consider preparation of $|110\rangle$, which requires instead local addressing on the rightmost atom.

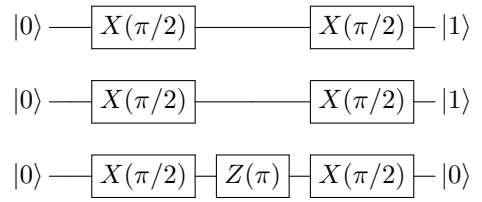

Local $X(\pi/2)$ for CNOT gate

To convert the $\mathcal{CZ}$ gate to the CNOT gate, we apply a local $X(\pi/2)$ before and after the gate to the target atom. We implement this as follows:

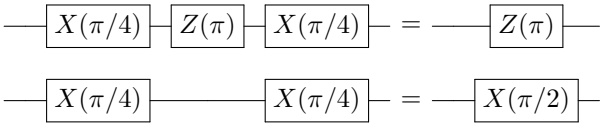

This circuit applies a local $X(\pi/2)$ on the right atom; while it additionally applies a $Z(\pi)$ gate on the left atom, this circuit is only applied in a context in which the left atom is in a computational basis state $|0\rangle$ or $|1\rangle$, in which case the $Z(\pi)$ gate only introduces a global phase and

therefore plays no role. In general, applying additional $Z(\pi)$ gates could be used to cancel the effect on the left atom, but this was not necessary for these experiments.

Local Hadamard for Toffoli implementation

To convert the CCZ gate to a Toffoli gate, we apply a local rotation on the target (middle) qubit before and after the CCZ pulse. The simplest method to accomplish this given our native gate set is to apply a global $X(\pi/4)$, followed by a local $Z(\pi)$ on the middle qubit, and then a global $X(3\pi/4)$.

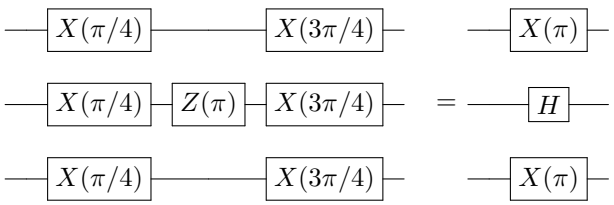

On each edge qubit, the net effect is simply a $X(\pi)$ gate. On the middle qubit, this sequence constitutes a Hadamard gate (defined along a different axis than the typical definition), where

$$H = \frac{1}{\sqrt{2}} \begin{pmatrix} 1 & i \\ -i & -1 \end{pmatrix} \tag{1}$$

DESIGN OF TWO-QUBIT CZ GATE

In this section we provide a detailed theoretical discussion of the two-qubit gate realized in the experiment. The desired unitary operation maps the computational basis states as follows:

$$\begin{aligned} |00\rangle &\to |00\rangle \\ |01\rangle &\to |01\rangle \\ |10\rangle &\to |10\rangle \\ |11\rangle &\to |11\rangle e^{i\pi} \end{aligned} \tag{2}$$

Up to a global gauge choice (i.e. global rotation of the qubits), this is equivalent to the following gate

$$\begin{aligned} |00\rangle &\to |00\rangle \\ |01\rangle &\to |01\rangle e^{i\phi_1} \\ |10\rangle &\to |10\rangle e^{i\phi_1} \\ |11\rangle &\to |11\rangle e^{i(2\phi_1+\pi)} \end{aligned} \tag{3}$$

where ϕ_1 is arbitrary.

To realize such a gate we drive both atoms globally and homogeneously with a laser that couples state $|1\rangle$ to the Rydberg state $|r\rangle$. This can be achieved via a single laser field or by a two-photon process. The Hamiltonian governing the dynamics of a pair of atoms is given by

$$H = \sum_{i=1}^{2} \frac{1}{2}(\Omega|1\rangle_i\langle r| + \Omega^*|r\rangle_i\langle 1|) - \Delta|r\rangle_i\langle r| + V|r\rangle_1\langle r| \otimes |r\rangle_2\langle r|$$

where Δ is the detuning of the excitation laser from the transition frequency between states $|1\rangle$ and $|r\rangle$, and Ω is the corresponding Rabi frequency. The interaction strength between two atoms in Rydberg states is given by V. In the following analysis we first assume that $V \gg |\Omega|, |\Delta|$, which can be realized by trapping the atoms sufficiently close to each other. This so-called Rydberg-blockade regime simplifies the following discussion, but is not crucial for the realization of the gate.

The dynamics of the system decouples into a few simple sectors:
(i) The state $|00\rangle$ doesn't evolve.
(ii) If one of the atoms is in $|0\rangle$, only the other system evolves. The dynamics is thus equivalent to that of a two level system (TLS) with states $|1\rangle = |a_1\rangle$ and $|r\rangle = |b_1\rangle$ and Hamiltonian

$$H_1 = \frac{1}{2}(\Omega|a_1\rangle\langle b_1| + \Omega^*|b_1\rangle\langle a_1|) - \Delta|b_1\rangle\langle b_1|.$$

(iii) If both atoms are initially in state $|1\rangle$, then the dynamics is again equivalent to that of an effective single TLS, formed by the states $|11\rangle = |a_2\rangle$ and $\frac{1}{\sqrt{2}}(|r,1\rangle + |1,r\rangle) = |b_2\rangle$, with Hamiltontian

$$H_2 = \frac{\sqrt{2}}{2}(\Omega|a_2\rangle\langle b_2| + \Omega^*|b_2\rangle\langle a_2|) - \Delta|b_2\rangle\langle b_2|.$$

This assumes a perfect Rydberg blockade, equivalent to $V \to \infty$. We stress again that this assumption simplifies the analysis but is not necessary to realize our proposed gate.

The controlled-phase gate can be constructed from two identical global pulses of the Rydberg laser field, with equal duration τ and detuning Δ, along with a phase jump by ξ in between. Each pulse changes the state of the atoms according to the unitary $U = \exp(-iH\tau)$. The change of the laser phase between pulses, $\Omega \to \Omega e^{i\xi}$, effectively corresponds to driving the system around a different axis on the Bloch sphere.

Let us examine how the four computational basis states evolve under the action of $\mathcal{U}$, which describes the effect of both laser pulses combined. First we note that $\mathcal{U}|00\rangle = |00\rangle$. Thus the unitary $\mathcal{U}$ maps the state $|00\rangle$ as expected for the CZ gate.

Next, let us consider the evolution of state $|11\rangle$. We choose the length of each pulse τ such that a system prepared in state $|11\rangle$ undergoes a complete, detuned Rabi oscillation and returns to the state $|11\rangle$ already after the first single pulse; that is, $U|11\rangle = e^{i\phi_2/2}|11\rangle$. This is guaranteed by the choice

$$\tau = 2\pi/\sqrt{\Delta^2 + 2\Omega^2}. \tag{4}$$

The second pulse also leads to a complete, detuned Rabi cycle about a different axis, but results in the same accumulated phase. In total, we find $\mathcal{U}|11\rangle = e^{i\phi_2}|11\rangle$. The dynamical phase accumulated by this process is given by $\phi_2 = 2\pi \times 2\Delta/\sqrt{\Delta^2 + 2\Omega^2}$.

Finally, let us consider the evolution of the states $|01\rangle$ and $|10\rangle$. In each case, this is also described by a detuned Rabi oscillation. However, due to the mismatch between the effective Rabi frequencies in H_1 and H_2, the state $|10\rangle$ ($|01\rangle$) does not return to itself after the time τ but a superposition state is created: $U|10\rangle = \cos(\alpha)|10\rangle + \sin(\beta)e^{i\gamma}|r0\rangle$, and $U|01\rangle = \cos(\alpha)|01\rangle + \sin(\beta)e^{i\gamma}|0r\rangle$. The real coefficients α, β and γ are determined by the choice of Ω, Δ and τ, and can easily be calculated (we omit explicit expressions here for compactness). Crucially, by a proper choice of the phase jump between the two pulses, ξ, one can always guarantee that the system returns to the state $|10\rangle$ ($|01\rangle$) after the second pulse. This can be calculated to be

$$e^{-i\xi} = \frac{-\sqrt{y^2+1}\cos\left(\frac{1}{2}s\sqrt{y^2+1}\right) + iy\sin\left(\frac{1}{2}s\sqrt{y^2+1}\right)}{\sqrt{y^2+1}\cos\left(\frac{1}{2}s\sqrt{y^2+1}\right) + iy\sin\left(\frac{1}{2}s\sqrt{y^2+1}\right)} \tag{5}$$

where we use the short hand notation $y = \Delta/\Omega$ and $s = \Omega\tau$. With this choice of the phase we thus have $\mathcal{U}|10\rangle = e^{-i\phi_1}|10\rangle$ and $\mathcal{U}|01\rangle = e^{-i\phi_1}|01\rangle$. The acquired dynamical phase can be calculated using straightforward algebra, and is a function of Δ/Ω, $\tau\Omega$ and ξ. Since we fixed τ in equation (4), and ξ in (5), ϕ_1 is actually solely determined by the dimensionless quantity Δ/Ω. Note that also ϕ_2 is only a function of Δ/Ω. However, the functional dependence is different, and we can find a choice for Δ/Ω such that $e^{i\phi_2} = e^{i(2\phi_1+\pi)}$ (see Fig. 2 of main text). With this choice, we obtain exactly the gate given in (3) which is equivalent to the controlled-phase gate (2) (up to trivial single qubit rotations). For completeness we give the corresponding numerical values of the relevant parameters:

$$\Delta/\Omega = 0.377371 \tag{6}$$

$$\xi = 3.90242 \tag{7}$$

$$\Omega\tau = 4.29268 \tag{8}$$

Finally, we note that this construction can be generalized to multi-qubit controlled phase gates in fully blockaded systems with more than two atoms.

Accounting for imperfect blockade

The above analysis is based on the perfect blockade mechanism. Finite blockade interactions (and other experimental imperfections, such as coupling to other Rydberg states) can be accounted for, and lead only to an effective renormalization of the parameters given in (6). To see this, note that a finite value of V only affects the dynamics if the system is initially in the state $|11\rangle$. Instead of being restricted to the two states $|a_2\rangle = |11\rangle$ and $|b_2\rangle = |1r\rangle + |r1\rangle$, a third state $|c_2\rangle = |rr\rangle$ has to be considered, and H_2 is replaced by

$$\begin{aligned} H_2 =& \frac{\sqrt{2}}{2}(\Omega|a_2\rangle\langle b_2| + \Omega|b_2\rangle\langle c_2| + \Omega^*|c_2\rangle\langle b_2| + \Omega^*|b_2\rangle\langle a_2|) \\ & - \Delta|b_2\rangle\langle b_2| + (V - 2\Delta)|c_2\rangle\langle c_2|. \end{aligned} \tag{9}$$

For $V \gg |\Delta|, |\Omega|$, the effect for finite blockade simply reduces to the two-level system $\{|a_2\rangle, |b_2\rangle\}$ where Δ is renormalized by an amount $\Omega^2/(2V)$. Even for small $V > 0$ and a given Δ, we can always choose Ω and τ such that the system initialized in the state $|a_2\rangle$ returns after the first pulse. Thus finite blockade simply replaces the complete Rabi oscillation in the fully blockaded regime, by a slightly more complicated, but still closed path in a two-dimensional Hilbert space. The analysis of the dynamics of the other computational basis states is unaffected by the finite value of V. It is thus straightforward to ensure that a system initially in the state $|10\rangle$ returns to $|10\rangle$ for each choice of V and Δ. This allows one to use Δ as a control knob for the relative dynamical phases acquired by $|11\rangle$ and $|10\rangle$, and thus realize a CZ gate.

EXPERIMENTAL CALIBRATION OF CZ GATE

The CZ gate requires two laser pulses with a relative phase shift between them. The detuning of the two pulses Δ is determined relative to the experimentally calibrated Rydberg resonance by numerical calculations. The pulse time and the phase jump between pulses both require experimental calibration due to perturbations in timing and phase asssociated with an AOM-based control system. The pulse time τ is calibrated first by preparing both atoms in the qubit pair in $|1\rangle$ and driving at detuning Δ to the Rydberg state. We observe detuned Rabi oscillations to the symmetrically excited state $|W\rangle = \frac{1}{\sqrt{2}}(|1r\rangle + |r1\rangle)$ and extract the pulse time at which the population returns fully to $|11\rangle$.

After fixing τ, we prepare only single isolated atoms in $|1\rangle$ and we drive two pulses of length τ with a variable relative phase. By identifying the phase for which the single atom returns fully to $|1\rangle$ by the end of the sequence, we fix the relative phase ξ.

Finally, we calibrate the global phase shift necessary to convert the CZ gate (with single-particle phase ϕ) into the canonical form:

$$\mathcal{CZ} = \begin{pmatrix} 1 & 0 & 0 & 0 \\ 0 & -1 & 0 & 0 \\ 0 & 0 & -1 & 0 \\ 0 & 0 & 0 & -1 \end{pmatrix} \tag{10}$$

We implement this phase correction by applying the global 420 nm laser for a fixed time in the absence of the 1013 nm Rydberg light; this avoids any resonant Rydberg excitation and instead only adds a phase shift. To

calibrate the phase correction, we apply the Bell state sequence in which we attempt to prepare the Bell state $|\Phi^+\rangle$ and then we apply an additional $X(\pi/2)$ rotation to both qubits. If our phase correction is optimal, we should prepare the state $|\Psi^+\rangle$, which we can measure in populations. We vary the global phase correction to maximize the measured populations in $|\Psi^+\rangle$ at the end of this sequence.

PREPARATION OF BELL STATE USING $\mathcal{CZ}$ GATE AND $\pi/4$ PULSE

Our global implementation of the $\mathcal{CZ}$ gate enables the preparation of Bell states with no local addressing. The protocol is most naturally understood by describing the two-qubit system in the Bell basis:

$$|\Psi^\pm\rangle = \frac{1}{\sqrt{2}}(|01\rangle \pm |10\rangle) \tag{11}$$

$$|\Phi^\pm\rangle = \frac{1}{\sqrt{2}}(|00\rangle \pm |11\rangle) \tag{12}$$

We prepare the system in $|00\rangle$, and after a global $X(\pi/2)$ pulse, we prepare the state

$$|\psi_1\rangle = \frac{1}{2}(|00\rangle - i|01\rangle - i|10\rangle - |11\rangle) \tag{13}$$

The controlled-phase gate creates the state

$$|\psi_2\rangle = \mathcal{CZ}|\psi_1\rangle = \frac{1}{2}(|00\rangle + i|01\rangle + i|10\rangle + |11\rangle) \tag{14}$$

$$= \frac{1}{\sqrt{2}}(|\Phi^+\rangle + i|\Psi^+\rangle) \tag{15}$$

The states $|\Phi^+\rangle$ and $|\Psi^+\rangle$ are both within the triplet manifold of the two qubits and are coupled resonantly by a global drive field to form an effective two level system with twice the single-particle Rabi frequency. A $\pi/2$ pulse within this effective two-level system corresponds to a $\pi/4$ pulse at the single-particle Rabi frequency, and maps:

$$|\psi_2\rangle = \frac{1}{\sqrt{2}}(|\Phi^+\rangle + i|\Psi^+\rangle) \rightarrow |\psi_3\rangle = |\Phi^+\rangle \tag{16}$$

IMPLEMENTATION OF CCZ GATE

We implement the controlled-controlled-phase (CCZ) gate in the regime in which nearest neighbors are constrained by the Rydberg blockade, but next-nearest neighbors have only weak interactions. In light of this, the CCZ gate that we aim to implement is motivated by the fact that both edge atoms can simultaneously blockade the middle (target) atom. In particular, we consider the following scheme to implement CCZ that involves local excitation to Rydberg states:

1. Apply a π pulse on both edge atoms, transferring all of their population in $|1\rangle$ to $|r\rangle$.
2. Apply a 2π pulse on the center atom, exciting from $|1\rangle$ to $|r\rangle$ and back to $|1\rangle$, accumulating a π phase shift only if neither edge atom is blockading this central atom and the atom is in $|1\rangle$.
3. Apply another π pulse on the edge atoms to return any population from $|r\rangle$ to $|1\rangle$.

Such a protocol realizes the following unitary:

$$\mathrm{CCZ} = \begin{pmatrix} 1 & 0 & 0 & 0 & 0 & 0 & 0 & 0 \\ 0 & -1 & 0 & 0 & 0 & 0 & 0 & 0 \\ 0 & 0 & -1 & 0 & 0 & 0 & 0 & 0 \\ 0 & 0 & 0 & -1 & 0 & 0 & 0 & 0 \\ 0 & 0 & 0 & 0 & -1 & 0 & 0 & 0 \\ 0 & 0 & 0 & 0 & 0 & 1 & 0 & 0 \\ 0 & 0 & 0 & 0 & 0 & 0 & -1 & 0 \\ 0 & 0 & 0 & 0 & 0 & 0 & 0 & 1 \end{pmatrix} \tag{17}$$

This unitary is equivalent to the canonical controlled-controlled-phase gate, denoted $\mathcal{CCZ} = \mathbb{1} - 2|111\rangle\langle 111|$ up to local rotations:

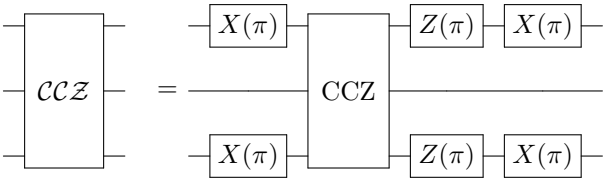

In the absence of local excitation to Rydberg states, we find that global Rydberg coupling can still approximately realize this unitary. Since different input configurations evolve according to dynamics of few-level systems with different coupling frequencies, it is challenging to design a single analytic global pulse to control all input configurations properly. For example, the $|001\rangle$ state couples to $|00r\rangle$ as a two-level system with Rabi frequency Ω. The $|011\rangle$ state couples to $\frac{1}{\sqrt{2}}(|01r\rangle + |0r1\rangle)$ with Rabi frequency $\sqrt{2}\Omega$. The $|111\rangle$ state couples both to $|1r1\rangle$ with Rabi frequency Ω, and also couples to $\frac{1}{\sqrt{2}}(|r11\rangle + |11r\rangle$ with Rabi frequency $\sqrt{2}\Omega$ (which then couples to $|r1r\rangle$). The systems are further complicated by the finite next-nearest neighbor interaction between edge atoms.

To find a global pulse that works on all input configurations, we use the RedCRAB optimal control algorithm [3, 4] to optimize an amplitude and frequency profile for the coupling field. The optimized pulse, shown in Fig. S3, has duration of 1.2 μs and achieves a numerically simulated gate fidelity of 97.6%.

Future experimental implementations with colder atoms could achieve higher gate fidelities by designing gate timings to intentionally cancel the effect of the unwanted phase accumulation between next-nearest neighbors. Alternatively, few-qubit gates could be implemented with all atoms in the fully blockaded regime by

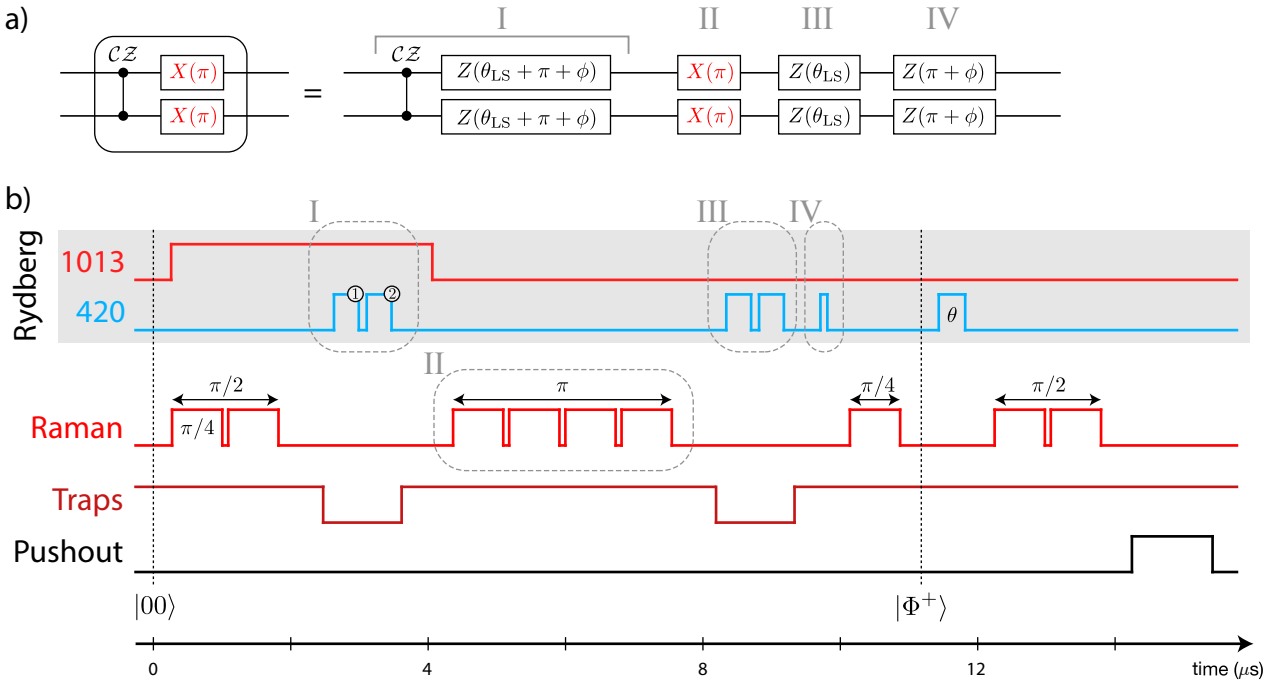

FIG. S2. **Detailed pulse sequences.** a) The implementation of the controlled-phase gate in the enclosed region (left hand side, as in main text Fig. 3), is shown in more explicit detail on the right hand side. The direct implementation of the $\mathcal{CZ}$ gate (region I) includes an extra phase shift on both qubits. This is corrected by a hyperfine qubit $X(\pi)$ echo pulse (II), followed by the appropriate phase shifts (III and IV). b) The full pulse sequence for preparing Bell states begins with both atoms in $|0\rangle$ and a global $X(\pi/2)$ pulse (produced by two $\pi/4$ Raman pulses) to put both atoms in $|-\rangle_y$. Then, while the 1013 nm laser is on, the 420 nm laser is applied in two pulses (with a relative phase between the pulses) to enact the CZ gate, along with global phase shifts coming from the light shift of the 420 nm laser. A global $X(\pi)$ pulse flips the qubit states, at which point the same 420 nm pulses are applied but now in the absence of 1013 nm light. This negates the effect of light shifts in the first portion of the CZ gate implementation. Then, an additional short pulse of the 420 nm laser adds an additional phase correction to turn the CZ gate into the canonical $\mathcal{CZ}$ gate. A subsequent global $X(\pi/4)$ pulse prepares the two atoms in the Bell state $|\Phi^+\rangle$. A final 420 nm laser pulse can be used to add dynamical phase to this Bell state, which can be detected by a subsequent global $X(\pi/2)$ for measuring parity oscillations. Finally, we push out atoms in $|1\rangle$ to detect populations.

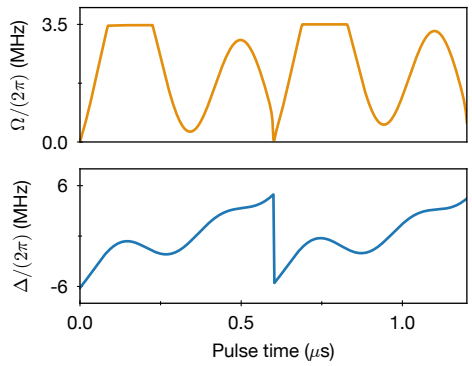

FIG. S3. **Optimal control pulse for CCZ implementation.** Time variation of Rydberg Rabi frequency and detuning to approximately implement the CCZ gate with numerically simulated fidelity 97.6%.

bringing atoms closer together or by exciting to higher Rydberg states.

ECHO PROCEDURE FOR CZ AND CCZ

The Rydberg pulse which implements the CZ or the CCZ gate includes both a 1013 nm laser field and a 420 nm laser field, the latter of which adds a differential light shift to the qubit levels of $\sim 2\pi \times 3$ MHz. To correct for the phase accumulated due to this light shift, after the CZ gate we apply a qubit $X(\pi)$ rotation on all atoms and then apply the same 420 nm pulse used for the CZ gate, but this time in the absence of 1013 nm light. The single particle phase ϕ (main text, eq. (1)) inherent in the design of the CZ protocol is separately corrected by an additional short pulse of the 420 nm laser. The full detailed pulse sequence is shown in Fig. S2.

STATE READOUT THROUGH ATOM LOSS

Our primary technique for state readout is to apply a resonant laser pulse that heats atoms in $|1\rangle$ (in $F = 2$, more generally) out of the tweezers, after which we take a fluorescence image of remaining atoms in $|0\rangle$. This

method correctly identifies atoms in $|0\rangle$, but can mistake atoms that were lost through background loss processes or by residual Rydberg excitation for atoms in $|1\rangle$, leading to an overestimation of the population in $|1\rangle$. For any measurements involving Rydberg excitation, we therefore collect measurement statistics both with and without the pushout pulse, which provides an upper bound on how much leakage out of the qubit subspace occurred, and therefore also gives a lower bound on the true population in $|1\rangle$.

We illustrate this procedure in the context of two-qubit experiments. Let us denote the two types of measurements as A (in which we apply the pushout of $|1\rangle$ atoms) and B (in which we disable the pushout). For each measurement procedure, we obtain statistics of observing the four two-qubit states, consisting of 'lost' or 'present' for each qubit. The A vector associates these as $|0\rangle$ and $|1\rangle$, so A_{ij} (for $i,j \in \{0,1\}$) denotes the probability of identifying the left and right atom in $0,1$ through the simple loss/presence analysis. However, the atoms can be not only in the qubit states $0,1$ but they can also be lost from the trap or in the Rydberg state, which in both cases will be detected as 'lost'. Let us denote C as the computational subspace containing $|0\rangle$ and $|1\rangle$, and denote $\overline{C}$ as anything outside this subspace (including Rydberg population or loss). The B vector measures whether the atoms are in C (either $|0\rangle$ or $|1\rangle$), or not ($\overline{C}$), so is denoted B_{ij} where $i,j \in \{C,\overline{C}\}$.

Both A_{ij} and B_{ij} can be explicitly expressed in terms of the underlying atomic populations $p_{\alpha\beta}$, where $\alpha,\beta \in \{0,1,\overline{C}\}$, as follows;

$$A_{00} = p_{00} \tag{18}$$
$$A_{01} = p_{01} + p_{0\overline{C}} \tag{19}$$
$$A_{10} = p_{10} + p_{\overline{C}0} \tag{20}$$
$$A_{11} = p_{11} + p_{1\overline{C}} + p_{\overline{C}1} + p_{\overline{C}\overline{C}} \tag{21}$$

$$B_{CC} = p_{00} + p_{01} + p_{10} + p_{11} \tag{22}$$
$$B_{C\overline{C}} = p_{0\overline{C}} + p_{1\overline{C}} \tag{23}$$
$$B_{\overline{C}C} = p_{\overline{C}0} + p_{\overline{C}1} \tag{24}$$
$$B_{\overline{C}\overline{C}} = p_{\overline{C}\overline{C}} \tag{25}$$

Measuring A_{ij} and B_{ij}, we can now solve for the atomic populations of interest: $p_{00}, p_{01}, p_{10}, p_{11}$.

$$p_{00} = A_{00} \tag{26}$$
$$p_{01} = A_{01} - B_{C\overline{C}} + p_{1\overline{C}} \tag{27}$$
$$p_{10} = A_{10} - B_{\overline{C}C} + p_{\overline{C}1} \tag{28}$$
$$p_{11} = A_{11} - B_{C\overline{C}} - B_{\overline{C}C} - B_{\overline{C}\overline{C}} + (p_{0\overline{C}} + p_{\overline{C}0}) \tag{29}$$

Since all probabilities are non-negative and $B_{C\overline{C}} + B_{\overline{C}C} + B_{\overline{C}\overline{C}} = 1 - B_{CC}$, we have our lower bounds for the true populations:

$$p_{00} = A_{00} \tag{30}$$
$$p_{01} \geq A_{01} - B_{C\overline{C}} \tag{31}$$
$$p_{10} \geq A_{10} - B_{\overline{C}C} \tag{32}$$
$$p_{11} \geq A_{11} - (1 - B_{CC}) \tag{33}$$

This is the analysis carried out for the Bell state populations, the CNOT truth table, and the Toffoli truth table (extended to three qubits). For the truth tables, the analysis is carried out for each measurement configuration (corresponding to a different input computational basis state) separately, shown as the rows in the matrices of Fig. S4.

CORRECTING FOR STATE PREPARATION AND MEASUREMENT ERRORS

We consider the problem of correcting a measured fidelity for state preparation and measurement (SPAM) errors. We denote P as the probability to correctly initialize and measure all qubits; generally, $P = (1-\epsilon)^N$ for single-particle SPAM error rate of ϵ. The measured fidelity is related to the 'corrected fidelity' according to:

$$\mathcal{F} = P \times \mathcal{F}^{\mathrm{c}} + (1-P) \times \mathcal{F}^{\mathrm{false}} \tag{34}$$

Here $\mathcal{F}^{\mathrm{false}}$ denotes the false contribution to the measured fidelity signal in cases in which SPAM errors occur. The main subtlety in performing this correction is properly evaluating the potential false contribution $\mathcal{F}^{\mathrm{false}}$.

Experimentally, the SPAM error is $\epsilon = 1.2(1)\%$ per qubit, consisting of two effects: first, the optical pumping into $|0\rangle$ has an error probability of $0.7(1)\%$, constituting a state preparation error. Second, there is a small chance that an atom can be lost due to a background collision either before or after the Bell state circuit is performed. Loss before the circuit contributes as a state preparation error; loss after the circuit but prior to the readout fluorescence image contributes as a measurement error. The total background loss contribution is $0.5(1)\%$ error per atom.

Bell state fidelity

The total probability that no errors occur on either of two qubits is $P = 97.6(2)\%$. Equation (34) holds for both the population measurement and the parity oscillation measurement separately. The population measurement explicitly only counts lower bounds on the population of atoms within the qubit subspace (see section: "State readout through atom loss"). Therefore, in cases where an atom is lost there is no false contribution to the measured fidelity. However, our measured fidelity does not distinguish between atoms pumped into magnetic sublevels outside of the qubit subspace. We estimate that

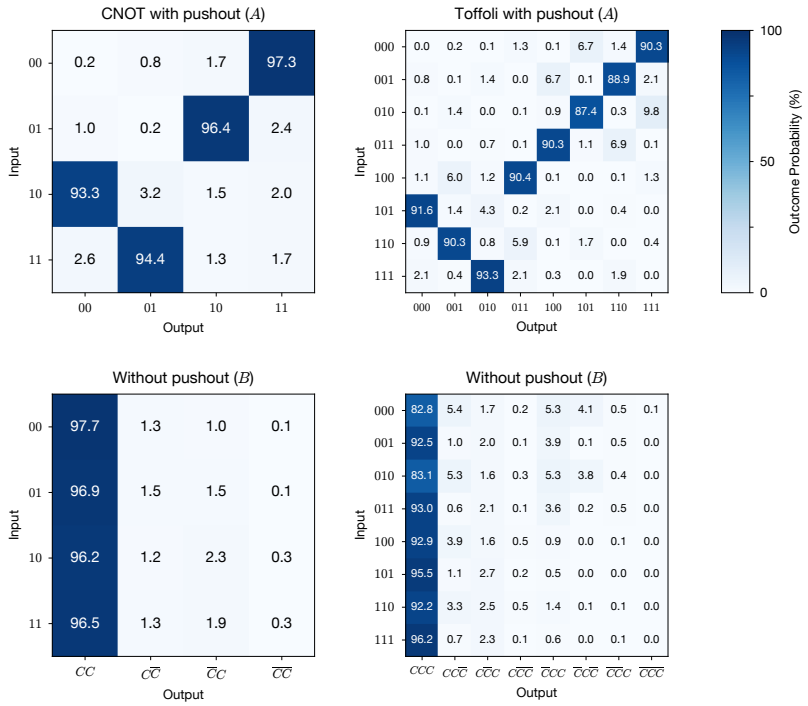

FIG. S4. Here we show full measurement statistics for the CNOT and Toffoli truth tables. In both situations, for each input computational basis state, we measure the probability distribution (shown in percentage points) of different output configurations both with and without the pushout pulse which removes $|1\rangle$ population, corresponding to the A matrix and B matrix, respectively. The output distribution of the A matrix is mainly associated with qubit levels $|0\rangle$ and $|1\rangle$ according to whether the atom is present or absent. However, this approach overestimates population in $|1\rangle$ since leftover population in the Rydberg state and losses due to other processes lead to the same measurement outcome as $|1\rangle$. To distinguish this effect, we measure without the pushout pulse (bottom row) to assess how much population is left in the computational subspace (C), rather than lost into the Rydberg state and therefore out of the computational subspace ($\overline{C}$). Comparing these two measurements provides a lower bound on the true atomic populations in the $|0\rangle$ and $|1\rangle$ qubit states.

in cases when one of the two atoms are prepared in an incorrect magnetic sublevel (1.4(2)% probability), there can be a false contribution of $\mathcal{F}^{\text{false}} = 1 - \cos^2(7\pi/8) \approx 15\%$ (calculated by evaluating the quantum circuit in the main text Fig. 3a with one atom not participating). The lower bound on the measured probablilities $p_{00} + p_{11} \geq 95.8(3)\%$ therefore set a lower bound on the corrected populations: $p_{00}^{\text{c}} + p_{11}^{\text{c}} \geq 97.9(4)\%$.

On the other hand, the parity oscillation amplitude receives no false contribution from cases when an atom is prepared in the wrong sublevel or is lost, because this error is independent of the accumulated phase and therefore does not oscillate as a function of the phase accumulation time. The false contribution is therefore $\mathcal{F}^{\text{false}} = 0$. In this case, the coherence C (given by the amplitude of the parity oscillation) is related to the corrected coherence by $C = P \times C^{\text{c}}$. Since $C = 94.2(4)\%$, we obtain a corrected coherence of $C^{\text{c}} = 96.5(4)\%$. The total SPAM-corrected Bell state fidelity, then, is $\mathcal{F}^{\text{c}} = \frac{1}{2}(p_{00}^{\text{c}} + p_{11}^{\text{c}} + C^{\text{c}}) \geq 97.2(3)\%$.

CNOT Truth Table

We measure the truth table by performing the CNOT gate on each computational basis state. The basis states are prepared with finite fidelity, as measured and shown in the main text Fig. 3e. For each basis state, we wish to assess how the finite output fidelity in the target state compares to the finite initialization fidelity to determine how well the gate performs on this input state. We establish a probability P_{ij} of no SPAM error occurring for each measurement setting (where ij denotes the setting in which we initialize the computational basis state $|ij\rangle$). Additionally, we measure a lower bound on the output probability in the target state, $\mathcal{F}_{ij}$.

We now consider false contributions to the measured fidelity. When an error involving atom loss occurs, there is no false contribution to fidelity since fidelity only measures atom population within the qubit subspace. Alternatively, in cases when the wrong computational basis state is prepared, then $\mathcal{F}^{\text{false}}$ is bounded

	Raw outcomes	Lower bound	Corrected
Bell state populations	97.6%	95.8%	97.9%
Bell state coherences	94.2%	94.2%	96.5%
Bell state fidelity	95.9%	95.0%	97.2%
CNOT: Input 00	97.3%	95.0%	96.5%
01	96.4%	94.9%	97.9%
10	93.3%	93.3%	96.3%
11	94.4%	93.1%	95.4%
CNOT Truth table	95.4%	94.1%	96.5%
Toffoli: Input 000	90.3%	73.1%	75.1%
001	88.9%	82.6%	86.2%
010	87.4%	73.0%	76.0%
011	90.3%	86.7%	90.0%
100	90.4%	84.3%	87.4%
101	91.6%	91.6%	95.7%
110	90.3%	87.0%	90.5%
111	93.3%	91.0%	95.0%
Toffoli Truth table	90.3%	83.7%	87.0%

TABLE S1. Summary of measurement results. Raw outcomes correspond to simple assignment of atom presence to qubit state 0 or 1. The lower bound comes from subtracting a conservative upper bound estimate on how much leakage out of the qubit subspace there may be, as determined by a separate measurement in which we do not push out $|1\rangle$ atoms. The corrected column shows the fidelities corrected for SPAM errors.

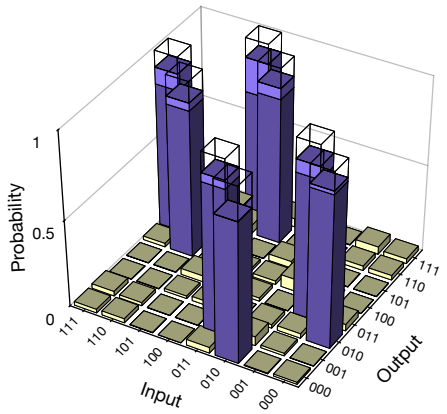

FIG. S5. **Limited tomography of Toffoli gate.** The raw target probabilities average to 88.0(3)%. Since four of the measurement configurations are precisely global $X(\pi)$ gates applied to the other four input states, we can compare these output distributions to properly account for leftover Rydberg population, similar to the procedure discussed in *State readout through atom loss*. We establish the limited tomography fidelity is therefore $\mathcal{F} \geq 81.5(5)\%$. Corrected for SPAM errors, the fidelity is $\geq 86.2(6)\%$.

above by the largest unwanted element of the truth table, or $< 4\%$. The total false contribution therefore is $(1-P) \times \mathcal{F}^{\text{false}} < (3\%) \times (4\%) \lesssim 0.1\%$. This contribution is below our measurement resolution and we do not account for it. The corrected fidelity is therefore just given by $\mathcal{F}^{\text{c}}_{ij} = \mathcal{F}^{\text{meas}}_{ij}/P_{ij}$. The average corrected truth table fidelity, given by the average of $\mathcal{F}^{\text{c}}_{ij}$, is therefore $\mathcal{F}^{\text{c}}_{\text{CNOT}} \geq 96.5\%$ (see Table S1).

Toffoli Truth Table

We perform the same analysis to evaluate the corrected Toffoli truth table fidelity as for the CNOT truth table. The average corrected truth table fidelity is $\mathcal{F}^{\text{c}}_{\text{Toff}} \geq 87.0\%$ (see Table S1).

LIMITED TOMOGRAPHY OF TOFFOLI GATE

The truth table of the Toffoli gate provides a representation of the magnitude of the matrix elements of the gate expressed in the logical basis. However, the measured populations carry no information about the relative phases between the different entries. Performing a similar procedure as the truth table but rotating the Toffoli gate to act on the X-basis instead of the Z-basis makes it possible to recover some information about these phases. A restricted version of such a procedure has been used before as a way to characterize the fidelity of the Toffoli gate [5], and has been dubbed "Limited Tomography". The procedure consists of initializing all the computational basis states in the Z-basis, and then applying an $X(\pm\pi/2)$ rotation to all qubits before and after a Toffoli gate. The sign is chosen to be $X(+\pi/2)$ when the target qubit is initialized in $|0\rangle$ and $X(-\pi/2)$ when the target qubit is initialized in $|1\rangle$.

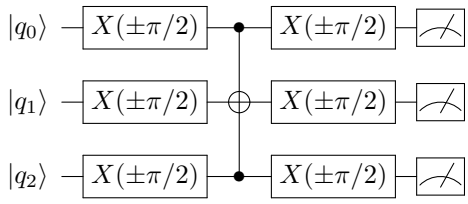

Conditioning the sign of the rotation on the state of the target qubit enforces that the target qubit is always in the same state $|+\rangle_y$ prior to the action of the Toffoli gate itself.

The Toffoli gate implemented in our system, which includes an echo pulse that acts as a global $X(\pi)$ gate (see main text, Fig. 4), is described ideally by the unitary matrix:

$$T_{\text{Ideal}} = \begin{pmatrix} 0 & 0 & 0 & 0 & 0 & i & 0 & 0 \\ 0 & 0 & 0 & 0 & 0 & 0 & 1 & 0 \\ 0 & 0 & 0 & 0 & 0 & 0 & 0 & -i \\ 0 & 0 & 0 & 0 & 1 & 0 & 0 & 0 \\ 0 & 0 & 0 & 1 & 0 & 0 & 0 & 0 \\ 0 & 0 & -1 & 0 & 0 & 0 & 0 & 0 \\ 0 & 1 & 0 & 0 & 0 & 0 & 0 & 0 \\ -1 & 0 & 0 & 0 & 0 & 0 & 0 & 0 \end{pmatrix}, \tag{35}$$

Performing the limited tomography procedure on this unitary should result in the following output truth table:

$$\text{Lim}[\text{T}_{\text{Ideal}}] = \begin{bmatrix} 0 & 0 & 1 & 0 & 0 & 0 & 0 & 0 \\ 0 & 0 & 0 & 1 & 0 & 0 & 0 & 0 \\ 1 & 0 & 0 & 0 & 0 & 0 & 0 & 0 \\ 0 & 1 & 0 & 0 & 0 & 0 & 0 & 0 \\ 0 & 0 & 0 & 0 & 0 & 0 & 1 & 0 \\ 0 & 0 & 0 & 0 & 0 & 0 & 0 & 1 \\ 0 & 0 & 0 & 0 & 1 & 0 & 0 & 0 \\ 0 & 0 & 0 & 0 & 0 & 1 & 0 & 0 \end{bmatrix}, \tag{36}$$

where each row shows the target output probabilities for a given input state. However, if the Toffoli gate is allowed to deviate from the ideal unitary by arbitrary phases ϕ_j according to

$$T_\phi = \begin{pmatrix} 0 & 0 & 0 & 0 & 0 & ie^{i\phi_1} & 0 & 0 \\ 0 & 0 & 0 & 0 & 0 & 0 & e^{i\phi_2} & 0 \\ 0 & 0 & 0 & 0 & 0 & 0 & 0 & -ie^{i\phi_3} \\ 0 & 0 & 0 & 0 & e^{i\phi_4} & 0 & 0 & 0 \\ 0 & 0 & 0 & e^{i\phi_5} & 0 & 0 & 0 & 0 \\ 0 & 0 & -e^{i\phi_6} & 0 & 0 & 0 & 0 & 0 \\ 0 & e^{i\phi_7} & 0 & 0 & 0 & 0 & 0 & 0 \\ -e^{i\phi_8} & 0 & 0 & 0 & 0 & 0 & 0 & 0 \end{pmatrix}, \tag{37}$$

then the limited tomography truth table reflects this phase deviation. In particular, each truth table matrix element in which the limited tomography should produce unity will instead result in a peak probability of $|\frac{1}{8}\sum_j e^{i\phi_j}|^2$. The average fidelity of the limited tomography truth table therefore reflects how close the phases on the Toffoli unitary are to their ideal values, and can only reach unity if each phase is correct. Our measured limited tomograpy truth table is shown in Fig. S5.

It is worth noting that the limited tomography protocol only makes use of four of the eight X-basis input states, as seen by the fact that the target qubit is always initialized in $|+\rangle$. This makes four out of the eight measurements equivalent to the other four up to a global $X(\pi)$ rotation at the end. Comparing these two sets of measurements gives a constraint on the probability of leakage out of the qubit subspace, similarly to the approach described in the section "State readout through atom loss."

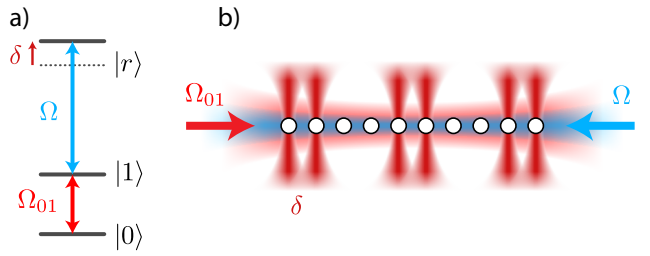

FIG. S6. Parallel gate implementation in a contiguous chain of atoms. (a) Local addressing lasers can shift the frequency of the Rydberg transition from $|1\rangle$ to $|r\rangle$ by δ without changing the $|0\rangle \leftrightarrow |1\rangle$ frequency. (b) The local addressing lasers are focused onto a subset of qubits on which we aim to perform parallel multi-qubit gates. The global Rydberg coupling laser is tuned to the light-shifted resonance, so that only the locally addressed atoms are coupled to the Rydberg state for gate implementation.

PARALLEL GATE IMPLEMENTATION IN A CONTIGUOUS ARRAY

The experiments performed here involve parallel multi-qubit gate implementation on separated pairs of atoms, where the inter-pair interaction is negligible. However, one can extend this protocol to parallel gate implementation in a contiguous chain of atoms, as illustrated in Fig. S6. We consider an additional local addressing laser system which can address an arbitrary subset of atoms, using for example an acousto-optic deflector. Specifically, one can select a wavelength for this laser such that the imparted light shift affects the $|0\rangle$ and $|1\rangle$ states equally, but differently from the Rydberg state $|r\rangle$. In such a case, the light shift from this new local addressing laser does not apply any qubit manipulations, but instead simply shifts the effective Rydberg resonance. Near-infrared wavelengths tuned far from any ground state optical transition ($\lambda \gtrsim 820$ nm) are suitable for Rubidium.

With such a system, we could illuminate all pairs of adjacent atoms on which we intend to perform two-qubit gates, and then by tuning the Rydberg laser to the light-shifted resonance we would perform the multi-qubit gate on all pairs in parallel. The only constraint is that there must be sufficient space between addressed pairs such that the interaction (cross-talk) between them is negligible in a particular layer of gate implementation.

[1] A. Omran *et al.*, "Generation and manipulation of Schrödinger cat states in Rydberg atom arrays," Science **365**, 570 (2019).

[2] H. Levine, A. Keesling, A. Omran, H. Bernien, S. Schwartz, A. S. Zibrov, M. Endres, M. Greiner, V. Vuletić, and M. D. Lukin, "High-fidelity control and entanglement of Rydberg-atom qubits," Physical Review Letters **121**, 123603 (2018).

[3] N. Rach, M. M. Müller, T. Calarco, and S. Montangero, "Dressing the chopped-random-basis optimization: A bandwidth-limited access to the trap-free landscape," Physical Review A **92**, 062343 (2015).

[4] R. Heck *et al.*, "Remote optimization of an ultracold atoms experiment by experts and citizen scientists," PNAS **115**, E11231 (2018).

[5] C. Figgatt, D. Maslov, K. A. Landsman, N. M. Linke, S. Debnath, and C. Monroe, "Complete 3-qubit Grover search on a programmable quantum computer," Nature Communications **8**, 1918 (2017).